J. Min. Metall. Sect. B-Metall. 54 (3) B (2018) 339 - 347

Journal of Mining and Metallurgy, Section B: Metallurgy

EFFECT OF MOLYBDENUM ADDITION ON HARDENABILITY OF CHROMIUM-BORON STEELS USED FOR PRESS HARDENING APPLICATIONS

M. Deepa*, G. Sahoo, S.K. Dhua

* R&D Centre for Iron and Steel, SAIL Ranchi, India

(Received 27 April 2018; accepted 09 August 2018)

Abstract

Two laboratory heats of low-Carbon low-alloy steels, one with boron and chromium additions and other with boron, chromium and molybdenum additions were made and cast into pencil ingots. These ingots were hot-rolled to 2 mm sheets suitable for press hardening application in an experimental rolling mill. A detailed study was made on the effect of various alloying elements on the microstructure and mechanical properties of these steels. A significantly higher hardness (~496 VHN), yield strength (~1137 MPa) and ultimate tensile strength (~1673 MPa) with comparable elongation (~6%) could be achieved in the as rolled and water-quenched Mo-Cr-B steel in comparison to Cr-B steel under similar processing condition. Moreover, a reduction of critical cooling rate by10°C/s was observed in this steel to obtain fully martensitic structure. The combined addition of boron, chromium and molybdenum was found to be more effective than that of boron and chromium in enhancing the microstructure and mechanical properties of boron-added steels. Additionally, a few hot compression tests were carried out to simulate the press hardening process of these experimental steels. It was found that one of the press hardening process parameters, viz., prior strain had a greater impact on the transformation behaviour of Cr-B and Mo-Cr-B steels during cooling.

Keywords: *Mo-Cr-B steel; Mechanical properties; Hardenability; Prior strain; Martensite*

1. Introduction

Since long, steel has been the material of choice for automakers worldwide and the automotive sector accounts for roughly 13% of the overall global steel consumption as per the estimation of the World Steel Association (WSA). With stringent regulations governing automobile emissions and fuel efficiency, automakers have been looking forward for steel with light weight and very high strength. Advanced high strength steels (AHSS) are considered to be the futuristic material in automotive sector. Unlike conventional deep-drawing grades, the AHSS steels exhibit more than 1500 MPa ultimate tensile strength and 1100 MPa yield strength on quenching. For this reason, researchers in steel industries have paid attention in alloying concepts and processing technologies on AHSS steels [1]. Boron steel is one of such advanced high strength steels, used for structural and impact resistance parts in automobile industry [2]. But such high strength steel also leads to an observable decrease in material formability. Due to high strength and low formability, advance high strength steels had limitations like larger spring back and early fracture. In order to enhance the forming limits of such high strength steel grades, automotive industries adopted advanced manufacturing methods in recent years. Press hardening is one of such innovative techniques for producing advanced high strength steel components like side impact and bumper beams by using boron steels. In this process, a blank is heated in a furnace in the austenitic region above 50°C of Ar3 temperature. Subsequently, it is transferred to the press for forming and quenching in a closed tool to obtain a fully martensite transformation in the material which cause an increase in tensile strength of up to 1500 MPa [3].

It is well known that the addition of a small amount of boron in steels significantly increases their hardenability on continuous cooling from austenite [4]. Boron addition of 10 to 30 ppm provides significant impact on the hardenability of low-carbon boron steel. The reason for increased hardenability is segregation of B atoms at the austenite grain boundaries which lowers the grain boundary energy resulting in the retardation of ferrite and pearlite nucleation [5]. Like boron, molybdenum in small quantity can also increase hardenability of steel [6, 7]. Moreover, the addition of Mo exhibits a combined effect in increasing the hardenability of B steels. The effect of combined additions of Mo and B has been investigated by many researchers in the past [6]. The

**Corresponding author:deepa@sail-rdcis.com*

DOI:10.2298/JMMB180427024D

effect of combined addition of Cr and B on the microstructure and mechanical properties of boron steel has also been studied by Abbasi et al. [8]. They reported that the critical cooling rate of 30°C/s was required to achieve fully martensitic structure.

Han et al. [6] investigated the effect of Mo and Cr separately on boron added steel and found Mo improved hardenability better than Cr. Asahi [7] proposed that M23(C, B)6 borocarbide formation at austenite grain boundaries was suppressed due to the combined addition of molybdenum and boron. Molybdenum had retarded carbon diffusion towards the austenite grain boundaries [7]. Investigation of Mo and B added steel with advanced techniques like atomic probe field ion microscope (AP-FIM) by researchers revealed the fine dispersive Ti-Mo carbonitrides (Ti,Mo)(C,N) and Mo-C clusters in as-rolled steels [9].

However, the synergistic effect of Mo and Cr in boron steels used for press hardening has not been investigated by any of the earlier researchers. Therefore, it was worth pursuing the present work to understand the combined effect of Mo and Cr additions on boron steel for improving strength as well as hardenability in press hardening grade steels. In addition, in the present study, the role of press hardening process parameters, particularly the effect of prior strain on the transformation behaviour of the experimental steels was also investigated [8].

2. Experimental

2.1 Laboratory heat making and hot-rolling

Two laboratory heats, 25 kg each, were made using a high frequency induction melting furnace. The melts were cast into 100 mm × 100 mm square ingots, which were subsequently hot-rolled to plates and sheets in an experimental rolling mill. Ingots were hot-rolled in two stages. In the first stage, the ingots were hot-rolled to 16 mm plates, while in the second stage, the 16 mm plates were hot-rolled to 2 mm sheets after soaking both at 1100°C for 120 and 60 minutes, respectively. The finishing temperature after hot-rolling was chosen in the range of 800 to 850°C. Phase diagram prediction with thermocalc revealed the presence of two phases at temperature below 800°C for both steel 1 and steel 2. The chemical composition of experimental steels (Table 1), all in wt%, was determined using M/s Bruker make Q8 Magellan 3440 model Optical Emission Spectrometer.

Table 1. *Chemical compositions of the experimental steels (wt. %)*

Steel	C	Mn	Si	B	Cr	Ti	Al	Mo	S	P
Steel 1	0.23	1.26	0.28	0.003	0.18	0.02	0.02	-	0.01	0.01
Steel 2	0.22	1.28	0.39	0.0035	0.18	0.05	0.05	0.09	0.018	0.013

2.2 Mechanical testing

Tensile test specimens were prepared as per ASTM A 370 standard with gauge length of 50 mm from 2 mm hot-rolled sheets of steels 1 and 2. Tensile tests were performed as per the above standard using UTM 7200, DAK system with cross head speed of 2 mm/minute, which is equivalent to strain rate 6.66 × 10-4 /s for 50 mm gauge length at ambient temperature. The hardness was measured in an Instron Wolpert Hardness Tester (Model: R Testor 643T). The tensile and hardness values are reported in Table 2.

Table 2. *Mechanical properties of as-rolled steels*

Steel	Condition	Hardness (VHN)	Yield Strength (MPa)	Ultimate Tensile Strength (MPa)	% Elongation	CE*
Steel 1	As-rolled & Air-cooled	169	350	598	13	0.32
Steel 1	As-rolled & Water-quenched	375	967	1207	6	0.32
Steel 2	As-rolled & Air-cooled	195	497	631	11	0.34
Steel 2	As-rolled & Water-quenched	496	1137	1673	5	0.34

2.3 Metallography

For light microscopy, specimens of steels 1 and 2 were cut from 2 mm sheets and ground successively from 100 to 1200 grit water proof silicon carbide paper and finally polished by using alumina suspension of particle sizes 1.0 µm and 0.3 µm. An optical microscope (Model: Olympus GX 71) was used for microstructural examination after etching the specimens in 2% Nital solution (98% alcohol + 2% nitric acid). The scanning electron microscope (Model: Zeiss EVO/MA 10) and the transmission electron microscope (Model: JEOL JEM- 2100) were used to distinguish the morphology of bainite and martensite, which were not clearly identified from the optical microscope. The samples for transmission electron microscope (TEM) were prepared by twin jet electro polishing technique. Initially, 3 mm diameter discs were punched from thin foils of nearly 0.1 mm thickness. Subsequently, the disc was subjected to twin jet electro-polishing using a mixture of electrolyte of 95% acetic acid and 5% perchloric acid. The thin perforated specimens were examined in transmission electron microscope at 200 kV operating voltage.

2.4 Dilation tests

A Gleeble-3500C model thermomechanical simulator with fully integrated digital closed loop control thermal and mechanical system was used for the dilation study. For this, 85 mm long cylindrical samples of 10 mm diameter were machined from the 16 mm thick hot-rolled plates. This experiment was designed to study phase transformation characteristics and critical parameters from the dilation plots. The schematic of the dilatometric cycle in this experiment is shown in Fig. 1. At first, the samples were soaked at 900 °C for 120s. Subsequently, the samples were cooled to room temperature at different cooling rates ranging from 1 to 30 °C/s. As reported by different researchers [10, 11], the austenization of B containing steels at higher temperature of austenization, especially above 900 °C, affects the effectiveness of B on hardenability due to the formation very hard and coarse high temperature boron compounds. On the other hand, the low temperature austenization will not much affect the solid solubility of Mo as Ti added to the experimental steels will tie of N to form TiN. This reduces the chances of formation of Mo(C, N) precipitate. This may be the reason for austenization of press hardening grade steel B steel around 900°C in industrial practice.

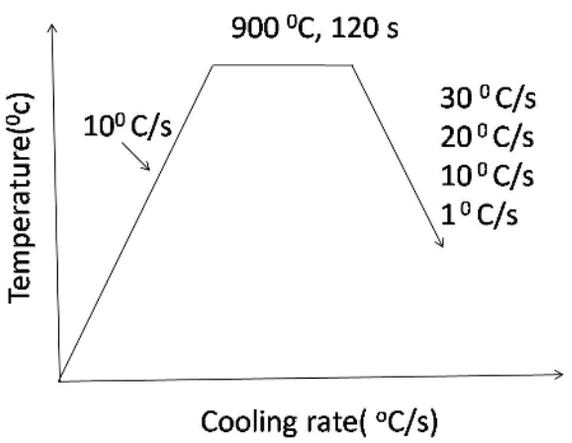

Figure 1. *Schematic illustration of dilatometry tests schedule*

2.5 Hot compression tests

In order to study the influence of deformation parameters, especially prior strain on transformation behaviour of steels 1 and 2, hot compression tests of isothermal forming were performed using thermomechanical simulator. The schematics of the isothermal process are provided in Fig. 2. For isothermal forming, the specimens were heated at the rate of 10 °C/s, soaked at 950 °C for 5 min and then cooled to the compression temperature of 800 °C at a cooling rate of 50 °C/s. The specimens were then isothermally deformed up to 50 % with a strain rate of 10/s followed by quenching at a cooling rate of 30 °C/s to ambient temperature.

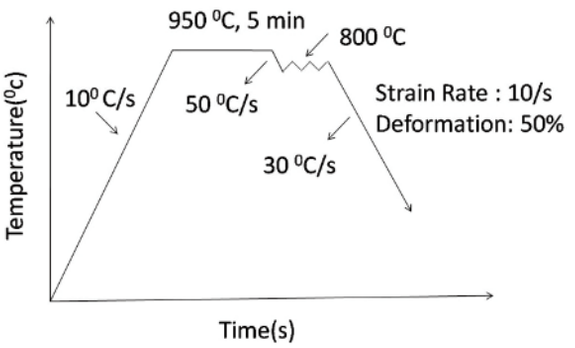

Figure 2. *Schematic illustration of hot compression test (Isothermal forming)*

3. Results and discussion

3.1 Alloy Design and Microstructure

As provided in Table 1, the compositions of both steels 1 and 2 were similar with respect to all elements except 0.09 wt. % Mo and an unintentional higher amount of Ti in steel 2. The carbon content in the range of 0.22-0.23 wt % was aimed to obtain optimum strength and ductility of martensitic boron grade steels used for press hardening purpose. The addition of Mn to commercial steels was always done for economic reasons in order to increase strength and hardenability. The other elements like B, Cr and Mo were added to increase hardenability of steels. Further, the aim was to discover their effects on final properties of experimental steels. The B content in these two steels was restricted to 35 ppm (max). Grossmann [12] reported that maximum effect of B on hardenability of steels can be obtained by restricting its content in the range of 30-35 ppm. Grange and Garvey [13] observed that nitrides act as nucleating agents in the decomposition of austenite, particularly for the formation of ferrite and thus, martensitic transformation is hindered. To suppress the BN formation, strong nitride-forming elements, such as titanium, were added in the range (0.02-0.04 wt%) in experimental steels for fixing nitrogen. According to Grossmann [12], the chromium content of 0.20 % increased the hardenability by about 50 % in commercial steel. The higher Cr content (> 0.20 %) may lead to the formation of chromium carbides, which is detrimental to hardenability.

The difference in elemental compositions can be clearly noticed from their microstructure (Fig. 3). Jarvinen et al. [14] reported that the initial microstructure of boron steel is important when the

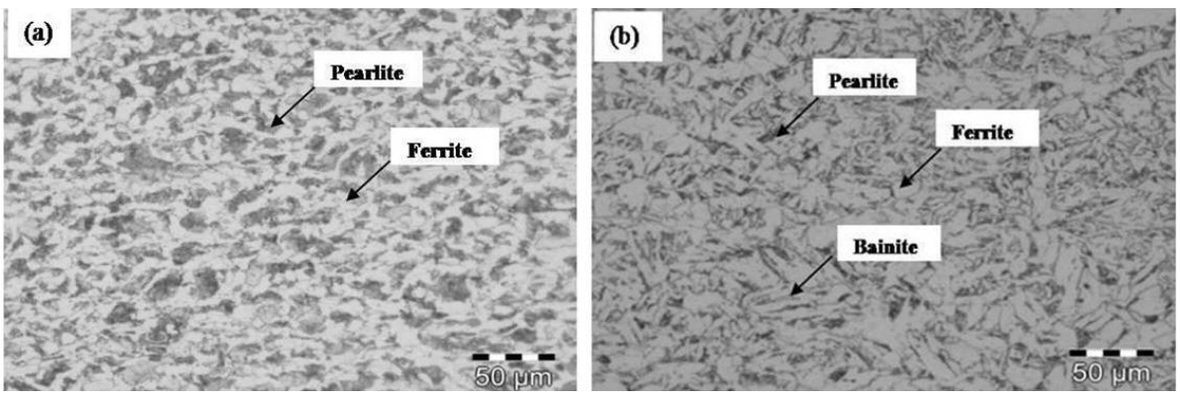

***Figure 3**. Optical photomicrographs after hot-rolling and air-cooling (a) steel 1 and (b) steel 2*

optimal mechanical properties are desired in the press hardening process. The process parameter of the direct press hardening process involves austenitizing, forming at higher temperature and quenching. After press hardening, a martensitic microstructure and tensile strength of 1500–1600 MPa are obtained. In addition, initial microstructure like parent austenite grain size also contributes significantly to obtain better mechanical properties. Fig. 3a and b showed the initial light micrographs of steels 1 and 2 respectively. While the former showed the presence of ferrite and pearlite, the later revealed the mixed microstructures of pearlite, bainite and ferrite. The observed microstructure of steel 1 with ferrite and coarse pearlite is in tune with the reported results in the literature [15]. The investigations on ultra-high strength steels by Karbasian et al [3] showed that boron alloyed steel initially exhibited a ferritic–pearlitic microstructure with a tensile strength of about 600 MPa. The composition of steel 2, however, enabled formation of bainite along with ferrite and fine pearlite after hot-rolling and air cooling as shown in Fig. 3b.

3.2 Hardness and Tensile Properties

Table 2 shows the hardness, tensile properties, e.g., yield strength (YS), ultimate tensile strength (UTS) and elongation percentage (%EL) of steels 1 and 2. The hardness, YS and UTS values achieved in steel 1 in as-rolled and water-quenched condition were 375 VHN, 967 MPa and 1207 MPa respectively, whereas, those were 496 VHN, 1137 MPa and 1673 MPa respectively for steel 2 under the similar processing condition. The enhancement of hardness, YS and UTS of steel 2 were found to be 121 VHN, 170 MPa and 460 MPa respectively with respect to steel 1 in this condition. The increase in hardness, UTS and YS of steel 2 can be related to its chemical composition, especially, to its carbon equivalent. The %El of steel 2 was found to be marginally lower in comparison to steel 1 (Table 2). Sung et al. [16] also reported an increase in strength and decrease in elongation with increasing CE or cooling rate. In addition to the alloying elements, variation in cooling rates can produce various microstructures in steels. Thus, the optimization of various chemical compositions and cooling conditions can enhance strength in steels. The higher carbon equivalent of steel 2 with respect to steel 1 should be enabled to achieve fully martensitic structure at lower cooling rate leading to its higher hardness and strength. The nominal lowering in percentage of elongation in steel 2 is attributed to its matrix hardening due to the addition of molybdenum.

3.3 Dilatometry and microstructure

Figs. 4 and 5 show the dilation curves and corresponding optical micrographs of steel 1 at different cooling rates, respectively while the TEM micrographs are shown in Fig. 6. In the case of steel 2, the dilatometric curves and optical micrographs at

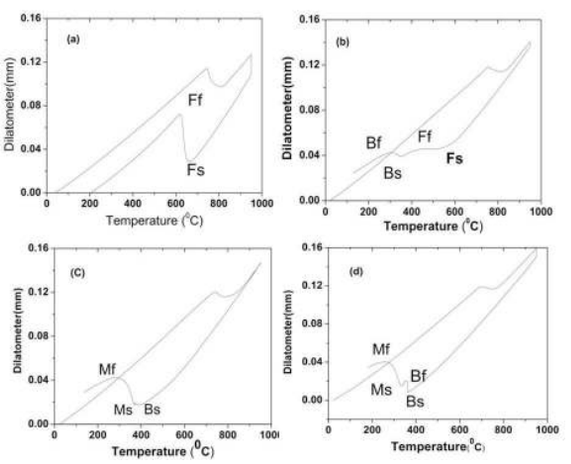

***Figure 4**. Dilatometric curves representing the phase transformation at cooling rate (a) 1 °C/s (b) 10 °C/s, (c) 20 °C/s, (d) 30 °C/s for steel 1.(Fs-ferrite start, Ff-Ferrite finish, Bs-Bainite start, Bf-Bainite finish, Ms-Martensite start, Mf-Martensite finish temperatures)*

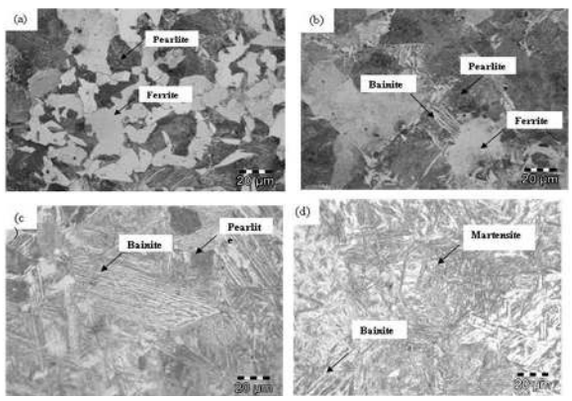

***Figure 5**. Optical microstructures of steel 1 at cooling rate (a) 1 °C/s (b) 10 °C/s (c) 20 °C/s and (d) 30 °C/s*

different cooling rates are shown in Figs. 7 and 8, respectively. The phase transformation temperatures were identified by considering the deviation of the curve from expected thermal contractions/expansions. The start temperature of pearlite to austenite transformation (Ac1 temperature) and austenite formation finish temperature (Ac3 temperature) is easily determined by dilatometric analysis. The phase transformations in steel are indicated with deviation from linear behaviour in the slope of a strain versus temperature plot [17].

The cooling part of the dilatometric curves of steel 1, as shown in Fig. 4a, depicts transformation at 682 °C for samples cooled at slower rates of 10 °C/s. The corresponding microstructure (Fig.5a) confirms the presence of ferrite and pearlite phase. Fig. 4b exhibits two stage transformations, one at 578 °C and other at 358 °C for samples cooled at the rate of 10 °C/s and the corresponding microstructure shown in Fig. 5b indicates the presence of both bainite and ferrite [18]. Fig. 4c depicts single stage transformations at 380 °C for sample cooled at the rate of 20°C/s and the corresponding microstructure shown in Fig. 5c exhibits presence of bainite. Fig. 4d also shows change in slope at two stages, bainite transformation at 367 °C and martensite transformation at 338 °C, which has been confirmed from the microstructures depicted in Fig. 5d at a cooling rate of 30°C/s. It is evident from the result that fully lath martensitic microstructure could not be achieved even at 30°C/s for steel 1.

TEM micrographs of steel 1 confirm the presence of upper bainite for sample cooled at the rate of 20 °C/s (Fig. 6a) and lower bainite for sample cooled at the rate of 30 °C/s(Fig. 6b) [19]. As shown in Fig. 6 (b), the incidence of needle-shaped carbides (Fe_3C) inside bainitic laths indicates its lower bainite configuration [20]. Further, the lower bainite morphology with single orientation observed in steel 1 is similar to that reported by Chang et al [21]. In the case of upper bainite, cementites are present at lath boundaries of ferrite while carbide is precipitated directly inside ferrite phase in the lower bainite. Both upper and lower bainite exhibits high dislocations inside ferrite phase in the experimental steels. Further, typical elongated precipitates was revealed (Fig. 6c) in steel 1 in the case of cooling rate of 30 °C/s. An energy dispersive spectroscopy (EDS) spectrum confirms presence of Cr and C resembling chromium carbides (Fig. 6d). The presence of other peaks related to Fe, Mn and Si has been attributed to the contribution of matrix surrounding the precipitates.

In the case of steel 2, the dilation curves (Fig. 7a) show that transformation occurs at 614 °C for sample cooled at slower rate of 10 °C/s. The optical microstructure of the corresponding dilated sample in Fig. 8a confirms the presence of ferrite and pearlite.

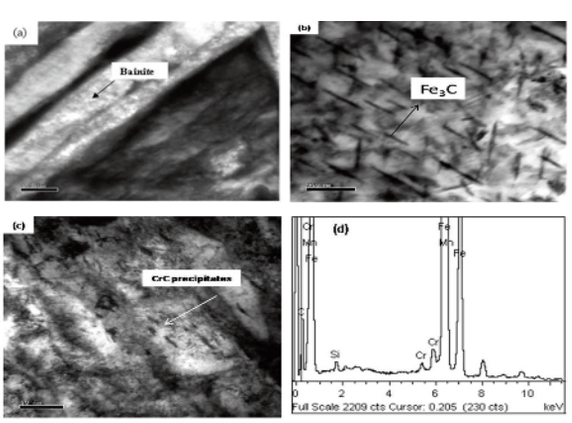

***Figure 6**. TEM micrographs of steel 1 showing (a) presence of alternate layers of ferrite and carbide indicating upper bainite at a cooling rate 20 °C/s (b) presence of iron carbides (Fe_3C) inside the laths indicating lower bainite at a cooling rate 30 °C/s (c) presence of elongated chromium carbide precipitates in lower bainitic structure (d) EDS spectrum taken on these precipitates showing Cr and C peaks*

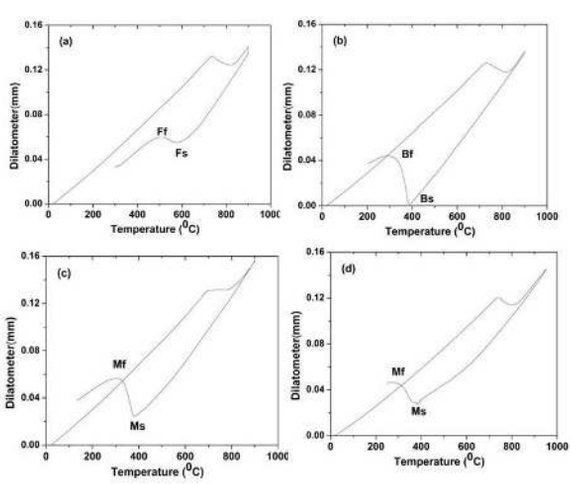

***Figure 7**. Dilatometric curves representing the phase transformation at a cooling rate (a) 1 °C/s (b) 10 °C/s (c) 20 °C/s (d) 30 °C/s for steel 2*

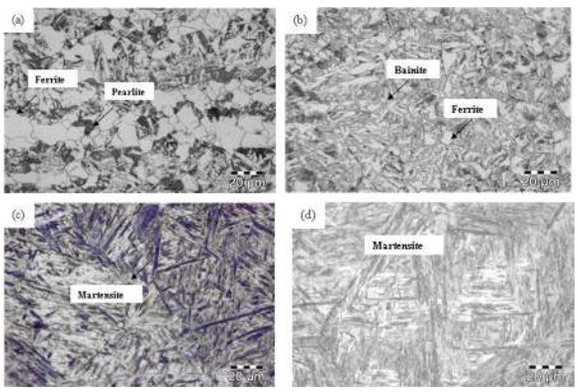

***Figure 8**. Optical microstructures of steel 2 (a) 1 °C/s (b) 10 °C/s (c) 20 °C/s and (d) 30 °C/s*

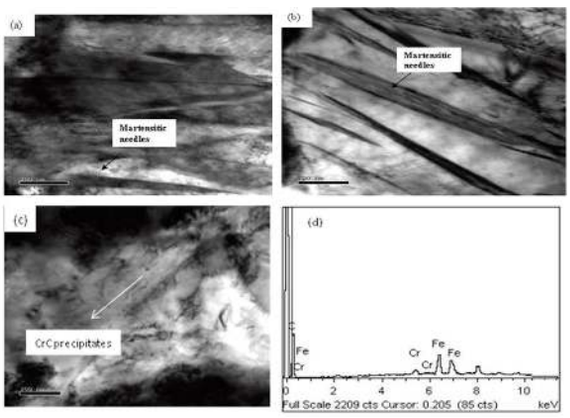

***Figure 9**. TEM micrographs for steel 2 at various cooling rates showing (a) presence of martensitic needles at a cooling rate 20 °C/s (b) presence of martensitic needles at cooling rate of 30 °C/s (c) presence of globular carbides (d) EDS spectrum of taken on these precipitates showing Cr and C peaks*

On the other hand, transformation occurs at 390 °C for sample cooled at the rate of 10 °C/s (Fig. 7b) and the corresponding microstructure in Fig. 8b confirmed incidence of bainite. Fig. 7c shows transformations at 372 °C for sample cooled at the rate of 20 °C/s. The corresponding microstructure in Fig. 8c shows the presence of martensite. On increasing further cooling rate to 30 °C/s, the transformation temperature was decreased to 350 °C (Fig. 7d) while the corresponding optical micrograph reveals fully martensitic microstructure as shown in Fig 8d.

The TEM micrographs of steel 2 subjected to the cooling rates of 20 °C/s and 30 °C/s are shown in Fig. 9a and b. The incidences of martensite needles both at the cooling rates of 20 °C/s and 30 °C/s were clearly evident. Unlike elongated precipitate observed in the case of steel 1 subjected to similar cooling rate, steel 2 only shows occasional globular precipitates. An EDS spectrum of a typical globular precipitate (Fig. 9c) shows elemental peaks of Cr and C related to chromium carbide precipitates as depicted in Fig. 9(d).

Fig. 10a and b show the effect of cooling rate on the transformation temperature and hardness of steels 1 and 2. It could be observed from Fig. 10a and 10b that in general the transformation temperatures were decreased with the increase of cooling rate, but, the bainite transformation temperatures (Bs) had little changes with cooling rate. The austenite to ferrite transformation temperature (Fs) of steel 1 is higher than that of steel 2. Presence of Mo in steel 2 decreased the ferrite start temperature [6]. Also, the hardness of steel 1 is lower than that of steel 2 at all cooling rates. The highest hardness was achieved for steel 2 at a cooling rate of 30 °C/s. Han et al. [6] reported the highest hardness of 375 HV of Mo-B steels at a cooling rate of 50 °C/s. However, the combined addition of Cr and Mo in steel 2 had increased the hardness to 512 HV at a cooling rate of 20 °C/s. Thus, the synergestic effect of both these

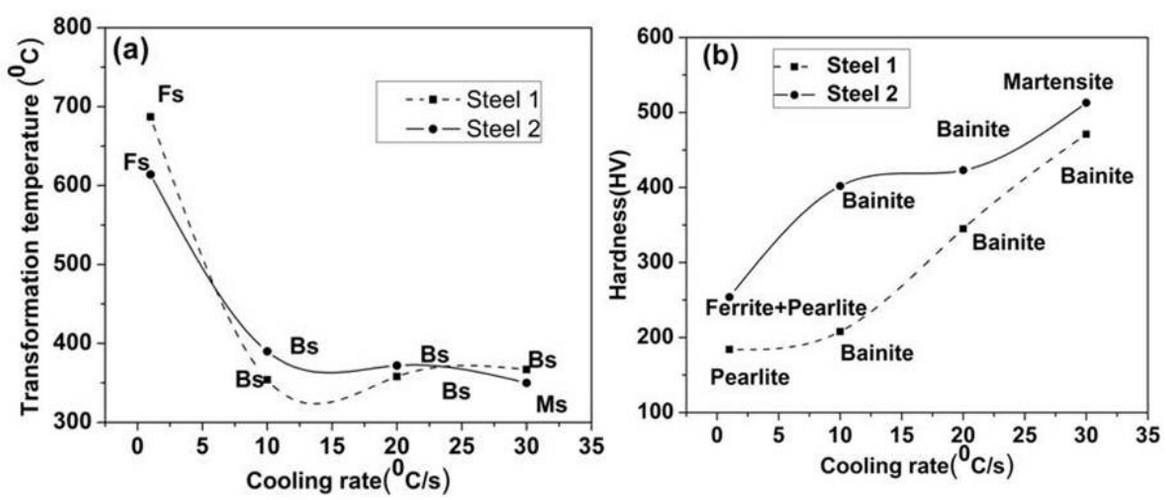

***Figure 10**. Effect of cooling rate on (a) transformation temperatures (b) hardness of steels 1 and 2*

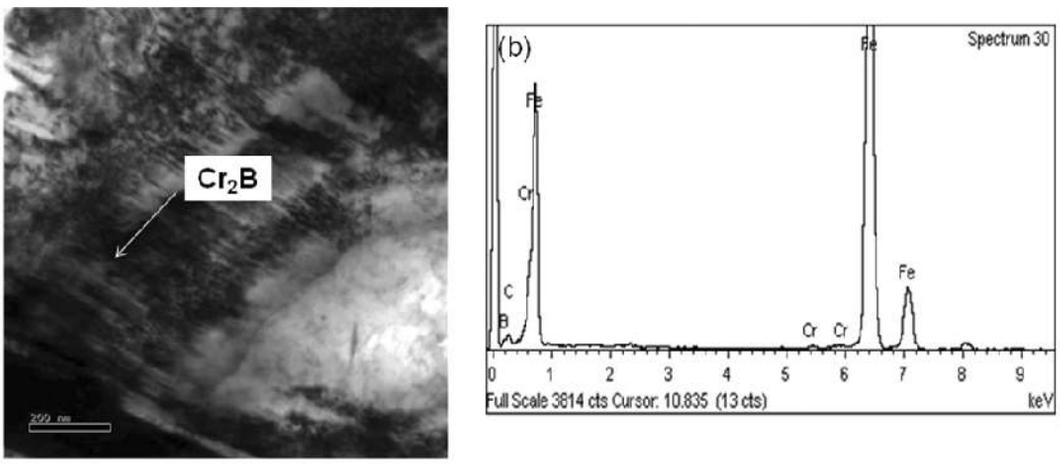

Figure 11. *TEM micrographs for steel 1 (a) Cr_2B at a cooling rate 30 °C/s (b) EDS spectrum of taken on these precipitates showing Cr and B peaks*

elements in increasing hardness was clearly noticed in this study.

In the case of steel 1, Fig. 11 shows the TEM micrographs and EDS spectrum of boride precipitates, especially of Cr, though large peaks of Fe were contributed from the matrix of surrounding precipitates. This boride precipitate was not found in steel 2 for which this was not presented in the manuscript. It is known from the literature that such borides in austenite grain boundaries deteriorates the hardenability [22]. In contrast to this, the recent work on Mo added Cr free boron steels reveals only the solute segregation (B, Mo, P, and Nb) at prior austenite grain boundaries, which has been attributed to their high binding energies with vacancies [20, 22, 23]. On the other hand, segregation of Cr and Mn at prior austenite grain boundaries was not reported as their binding energies with vacancies was low [23]. Further, during cooling after martensite formation, the extremely supersaturated martensite with all remaining solutes such as C, Si, Mn, and Cr enhanced the total system free energy. Hence the reduction of the energy acted as a driving force for solute segregation to martensite lath boundaries. Therefore, both Mo and B segregation in prior austenite grain boundaries and remaining solutes segregation in martensite lath boundaries enhanced the hardenability in steel 2 [24]. In contrast to this, the formation of borides resulted in decrease in soluble B at prior austentite grain boundary and enhanced the ferrite formation [6,7], which lead to lesser hardness of steel 1. To quantify B and other alloying elements (C, Cr, Mo) at prior austenite grain boundaries and in the matrix, a detailed investigation will be carried out using atom probe tomography in future study. Atom Probe Tomography (APT) is essential for fundamental understanding of grain boundary segregation and it also gives precise information on solute distribution at the atomic scale.

3.4 Hot compression tests and microstructure

Optical microstructures at undeformed conditions of steels 1 and 2 are shown in Figs. 12a and 13a. On the other hand, the Figs. 12b and 13b show the optical images of these steels after isothermally deformed up

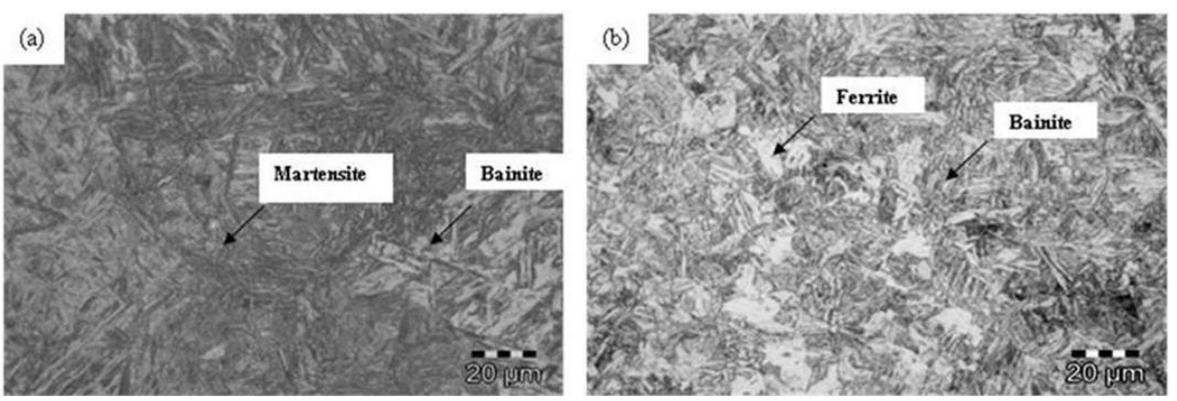

Figure 12. *Optical microstructures of steel 1(a) Undeformed, cooled at a rate of 30 °C/s to ambient temperature (b) Deformed upto 50% and cooled at a rate of 30 °C/s to ambient temperature*

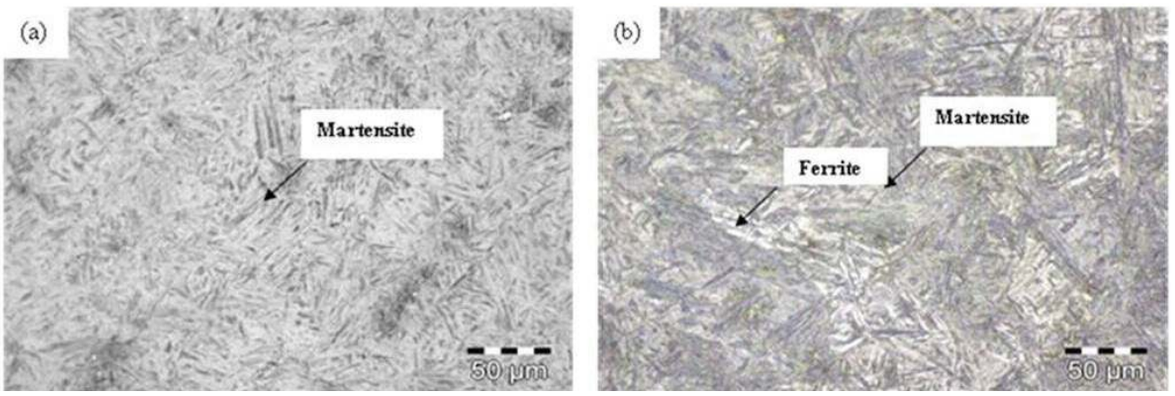

Figure 13. *Optical microstructures of steel 2 (a) undeformed and (b) deformed (50%) during isothermal treatment at 800°C followed by cooling at the rate of 30 °C/s*

to 50% at 800°C, followed by fast cooling at the rate of 30 °C/s. On comparing these micrographs in both conditions, it is inferred that the deformation conditions had promoted the ferrite formation along with martensite in steels 1 and 2. Somani et al. [25] also observed enhancement of ferrite formation by plastic deformation of austenite in microalloyed steel.

TEM micrographs of both steels 1 and 2 shown in Fig. 14 also reveal the presence of ferrite. According to Barcellona et al. [26], increasing hot deformation promoted ferrite formation, which was also observed in the present case both in steels 1 and 2. The experimental results indicated that increasing hot deformation amounts shifts the CCT diagram toward lower times.

It was also reported that even high temperature prestrain of 8% at 800°C quenched at higher cooling rate produced higher amount of ferrite and pearlite phases for boron alloyed steels [26]. Somani et al. [25] also observed strain induced ferrite formation after plastic deformation. The experimental results gave evidence that minimization of the plastic strain and maximization of the cooling rate were suitable ways to avoid excessive ferrite formation. The desired martensitic microstructure in formed and quenched components was possible with a control of prestrain and cooling rate. However, to get the desired microstructure and the mechanical properties of the material under different hot deformation conditions, further investigation needs to be carried out.

4. Conclusions

1. The addition of Mo in Mo-Cr-B steel increased its hardness, YS and UTS significantly in comparison to Cr-B steel. The hardness, YS and UTS of steel 2 was increased by 121 VHN, 170 MPa and 460 MPa respectively with respect to steel 1, in as-rolled and water quenched condition.
2. Due to synergy of Mo and Cr, Mo-Cr-B steel had a fully martensitic structure desirable for press hardening at a cooling rate of 20 °C/s, whereas, Cr-B without Mo had bainitic structure at the same cooling rate. Hence, the cooling rate to achieve fully martensitic structure was lowered by10 °C/s in steel 2.
3. The prior strain during isothermal treatment had been found to alter the transformation characteristics of both Cr-B and Mo-Cr-B steels. In both Cr-B and Mo-Cr-B steels, martensitic transformation was suppressed when they were deformed 50% during

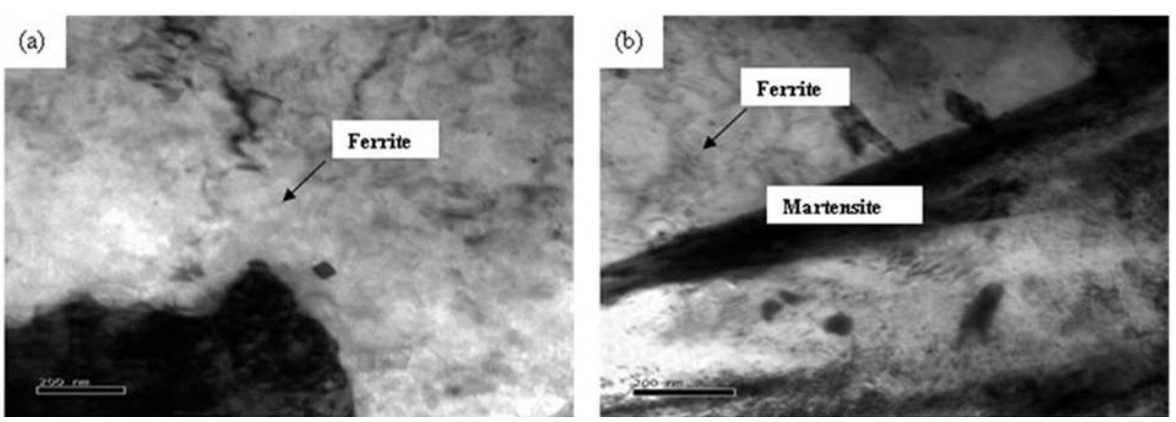

Figure 14. *Bright Field TEM micrographs showing (a) Ferrite formation in steel 1 and (b) Ferrite formation in steel 2, both deformed (50%) during isothermal treatment at 800°C followed by cooling at the rate of 30 °C/s*

isothermal treatment at 800ºC, followed by cooling at the rate of 30 ºC/s up to the ambient temperature. Prior deformation decreased the martensite formation both in Cr-B and Mo-Cr-B steels.
4. Therefore, the prior strain at this level proved to have adverse effect on the martensitic transformation in the experimental steels. The martensitic fraction decreased when prior deformation was present before cooling in experimental steels.

Acknowledgement

The authors are thankful to the management of R&D Centre for Iron & Steel, Steel Authority of India Limited for their support for carrying out this work and giving permission for publishing the same.

References

[1] T. Nonaka, K. Goto, H. Taniguchi, K. Yamazaki, Development of ultra high strength cold rolled steel sheets for automotive use, Nippon Steel technical report.88, 2003,p 13 – 15.
[2] Altan,T., Yadav,A. (2007) Press hardnening Boron-alloyed Steels for Automotive Parts – Part II, Stamping Journal.
[3] H.Karbasian, A.E.Tekkaya, J. Mater. Process. Techno, 210 (2010) 2103–2118.
[4] C.R. Simcoe, A.E. Elsea, G.K. Manning, Trans. Soc. AIME, (1956) 984-988
[5] J.E. Morral, T.B.Cameron, Met. Trans. A, 8A (1977) 1817-1819
[6] F. Han, B. Hwang, D-W. Suh, Z. Wang, D.L. Lee, S-J. Kim, Met and Matals Intl, 14 (2008) 667-672.
[7] H. Asahi, ISIJ inter, 42 (2002) 1150-1155.
[8] M.Abbasi, A.Saeed-Akbari, M.Naderi, Mater. Sci. Eng. A, 538 (2012) 356–363.
[9] J. Takahashi, K. Ishikawa, K. Kawakami, M. Fujioka, N. Kubota, Acta Materialia. 133 (2017) 41-54.
[10] S.W.Tanabe, H. Ohtani, Transactions ISIJ 23 (1983) 38-42.
[11] J. A. Jimnez, P. Adeva, M. C. Cristina and O. A. Ruano, Mater. Sci. and Eng. A 159 (1992) 103-109
[12] M.A Grossmann, AIME 1437 (1942) 1-29.
[13] R. A. Grange and T. M. Garvey, Trans. Am. Soc. Metals 37 136 (1946)
[14] H. Jarvinen, M.Isakov, T Nyyssonen , M. Jarvenpaa, P.Peura, Mater. Sci. Eng. A 676 (2016) 109–120.
[15] M. Naderi, M. Ketabchi , M. Abbasi, W. Bleck, steel research int. 81 (2010) 216-223.
[16] H K Sung, S. Y Shin, B. Hwang, C. G Lee, N J. Kim, S.Lee, Mater. Sci. Eng. A 530 (2011) 530–538.
[17] A.Grajcar, W. Zalecki, P. Skrzypczyk, A. Kilarski, A. Kowalski, S. Kołodziej, J. Therm. Anal. Calorim. 2 (2014) 739-748.
[18] A. Kamyabi-Gol, S.J. Clark, J.W Gibbs, S. Sridar, P.F. Mendez, Acta Materialia 102 (2016) 231-240.
[19] Zhi-Gang Yang, Curr Opi. in Solid Sta and Mats. Sci. (2005) 277-280.
[20] H. Bhadeshia, R Honeycombe, Steels: Microstructure and Properties: Bainite 2017, Elsevier Ltd, UK, 179–202.
[21] L.Chang, H.K.D.H.Bhadesia, J.Mater.Sci 31 (1996) 2145-2148.
[22] Y.S. Choi, S.J. Kim, I.M. Park, K.W. Kwon, I.S.Yoo, Met. Mater. Int. 3 (1997) 118-124.
[23] Y.J.Li , D.Ponge ,P.Choi, D.Raabe , Ultramicroscopy. 159 (2015) 240-247.
[24] Y.J.Li, D.Pong, P.Choi, D.Raabe, Scr. Mater. 96 (2015) 13–16.
[25] M. C. Somani, L. P. Karjalainen, J. Mater. Sci. Technol. 17 (2001) 203-206.
[26] A.Barcellona, D.Palmeri, Metall. Mater. Trans. A 40 (2009) 1160–1174.

UTICAJ DODAVANJA MOLBIDENA NA OČVRŠĆAVANJE ČELIKA SA DODATKOM HROMA I BORA KOJI SE KORISTI ZA POSTUPKE VRUĆEG PRESOVANJA

M. Deepa*, G. Sahoo, S.K. Dhua

* R&D Centar za gvožđe i čelik, SAIL Ranči, Indija

Apstrakt

Dva laboratorijska uzorka niskolegiranog čelika sa malim sadržajem ugljenika, prvi sa dodatkom bora i hroma, a drugi sa dodatkom bora, hroma i molbidena, napravljena su i izlivena u četvrtasti ingot (odlivak). Ovi ingoti su valjani u toplom stanju dok nisu dobijeni limovi debljine 2mm koji su pogodni za postupke vrućeg presovanja u eksperimentalnim valjaonicama. Detaljno su ispitani uticaji različitih legirajućih elemenata na mikrostrukturu i mehaničke osobine ovih uzoraka čelika. Značajno viša tvrdoća (~496 VHN), napon na granici tečenja (~1137 MPa) i zatezna čvrstoća (~1673 MPa) sa relativnim izduženjem (~6%) mogu se postići kod Mo-Cr-B čelika dobijenog valjanjem na taj način i kaljenim u vodi u poređenju sa Cr-B čelikom pod sličnim uslovima tokom postupka. Osim toga, uočeno je i smanjenje kritične brzine hlađenja za 100C/s kod ovog uzorka za dobijanje potpune strukture martenzita. Dodavanje kombinacije bora, hroma i molibdena je efektnije nego dodavanje samo bora i hroma za mikrostrukturu i mehaničke osobine čelika sa dodatkom bora. Pored toga, izvedeno je i nekoliko ispitivanja materijala na pritisak u toplom stanju da bi se simulirao postupak kaljenja pod presom ovog eksperimentalnog čelika. Došlo se do zaključka da je jedan od parametara ovog postupka, prethodno istezanje, imao veći uticaj na transformaciju Cr-b i Mo-Cr-B čelika tokom hlađenja.

Ključne reči: *Mo-Cr-B čelik; Mehaničke osobine; Otvrdnjavanje; Prethodno istezanje; Martenzit.*